A NEW DESIGN CODE FOR 1.5 Mwt HELIUM HEAT EXCHANGER

M. KITAGAWA, J. HAMANAKA, T. UMEDA, T. GOTO, Y. SAIGA
Ishikawajima-Harima Heavy Industries Co., Ltd.,
Research Institute, 1-15, Toyosu 3-chome, Koto-ku, Tokyo 135, Japan

M.OHNAMI
Ritsumeikan University Kyoto, Kyoto, Japan

T. UDOGUCHI
Chiba University, 1-33 Yayoi-cho, Chiba, Japan

SUMMARY

There is the ASME B & PV code for design criteria of high temperature heat exchanger and these design codes cannot be applied to the 1.5 Mwt Heat Exchanger System because the codes applying range are limited up to 815°C, while the new heat exchanger system is supposed to be operated at the temperatures upto 1000°C. Because this heat exchanger is a test loop for nuclear direct steal making plant, its design and construction requires as much safety assurance as the nuclear power plant.

In order to satisfy safety requirement, a new design code specifying heat exchanger components operable at a maximum allowable temperature of 1,000°C was proposed.

The code is essentially an expansion of the ASME B & PV code case 1592 and accepted by the committee, consisting of professors and researchers from universities, national research institutes, and private industrial companies.

The materials for high temperature components allowed in the new code are Inconel 617 and Hastelloy X. The components which will be subjected to the temperature below 800°C is recommended to be designed using the ASME B & PV Code Section III and Code Case 1592.

In order to make the design possible at such a high temperature as 1,000°C under new design code, some modifications and additions for the ASME code had to be made and substantiated by theoretical and experimental researches such as the development of detailed stress-strain analysis methods, the development the symplified elasto-plastic analysis method, various types of material strength research and simplified model strength analysis.

The effects of helium gas, welding, cold work, biaxiality, aging and heat treatment on the high temperature strengthes were determined experimentally. The most significant effect of the helium gas was found to be decarburization and carburization. The decarburization due to a helium gas (4-nine purity) decreased the creep strength significantly, although the fatigue strength in the helium was higher than in air. The cold work decreased or increased the creep strength depending on the amount of cold work, temperature and length of creep time. The creep ductility of tube under internal pressure was as low as 3 $\sim$ 5%. All of these high temperature material strengthes were reflected in the determination of allowable stresses.

The tertiary creep at the high temperature often starts earlier, unlike at elevated temperature. Therefore, a temporary new method of determining the S_t values which did not depend on the tertiary creep commencement was proposed. The buckling safety factor was increased to prevent the early tertiary creep. The thermal ratchet design method in the new code properly accounts for the temperature dependence of yield strength. Detailed design procedures for creep-fatigue evaluation, piping analysis, and elastic follow-up analysis were added.

1. INTRODUCTION

The ASME B & PV Code, Section III is a non-creep temperature code. The ASME B & PV Code Case 1592 gives design procedures for components which are used at the temperature in the creep range but only below 815°C. Design procedures for the temperatures above 800°C (referred to as high temperatures in this paper) had not been yet fully developed.

The authors have been engaged in the establishment of the design code for the 1.5 Mwt helium-to-helium heat exchanger system. A new design code is applicable for the heat exchanger components operable at a maximum temperature of 1000°C.

The purpose of this paper is to present some typical high temperature material properties of Inconel 617 and the method of reflecting these properties in the design codes.

2. BACKGROUND OF THE DESIGN CODE FOR HIGH TEMPERATURE HELIUM HEXT EXCHANGER

In order to obtain the data for the design stress intensities and to support the design procedure in a new code, a series of high temperature strength experiments, as shown in Table 1, were performed on Inconel 617 at 800 1000°C. Experimental works include various material strength tests and simplified model tests. In the followings, the result of material strength tests and their relation to the new design code shall be discussed. Because of the space limitation, some details shall be neglected and only typical data shall be shown.

2.1 MATERIAL SPECIFICATION

High temperature properties are known to vary widely depending on the minor variation of metallurgical structure. The relations among creep and mechanical properties, chemical composition and grain size of Inconel 617 were analysed using the corelation coefficient technique.

The results indicate that the variation of grain size and carbon content most affect the creep and mechanical properties of Inconel 617. Figure 1 shows an example of the relationship between creep rupture time (under 3.5 kg/mm^2 at 1000°C) and grain size. In order to limit the minimum creep strength in a reasonable lower limit, only the material with grain size of ASTM number 3 or coarser was decided to be allowed in new code.

2.2 THE EFFECT OF COLD WORK, WELDING, AGING AND ENVIRONMENT

The Code Case 1592 states that the material properties altered by environmental effect and by the effect caused by welding or cold work etc. should be accounted in the design but presentley these effects are not reflected in the design stress intensities.

The new design guide reflects the change of the material strength due to above effects using the so-called "material strength reduction factor, K_i". The design stress intensities is derived by the following equation.

$$S = K_i \; S^o$$

S^o is the design stress intensities for the solution annealed base metal in Air.

K_i is the strength reduction factor for a fracture mode i.

Figure 2 shows an example of strength reduction factor for an Ni-base superalloy Inconel 617 associated with the 4-nine purity helium gas. The effect of helium gas at high temperatures alters significantly with a small amount of inpurity variation. Figure 2 shows the K_i factor which is considered to be the lowest values among the values for the helium gas of various inpurity. This lowest value was used in our design of an intermediate helium heat exchanger of 1000°C, so as to be conservative as much as possible.

Figure 3 shows the isochronous stress-strain curves of Inconel 617 at 1000°C in helium gas which was calculated from isochronous stress-strain curves in air and the strength reduction factor given in Fig. 2. The figure also includes some experimental data which agree fairly well with the calculation.

An example of the effect of cold work on the creep strength is shown in Fig. 4. It is seen that the creep strength is altered by cold work. Based on the experimental results such as shown in Fig. 4, the heat treatment requirement for the heat exchange tubes was determined.

2.3 THE STRAIN LIMIT

Rupture or fracture ductility of all the creep ruptured specimens and short time tensile specimens was examined. The rupture strain in the bursted tubes was determined from the change in the wall thickness. In general, the fracture ductility of short time tensile was much higher than the ductility of creep ruptured specimens.

Figures 5 and 6 show examples of the fracture ductility of Inconel 617. It was found that the aging at 1000°C did not significantly reduce the ductility, but that the creep deformation had decreased the ductility noticeablly. Figure 7, which shows the strain distribution along the circumference of the creep ruptured tubes of Inconel 617, implies that the microvoids may appear at the strain of as small as 3 5%.

Based on the above experimental results, the accumulated strain allowed in our design guide was determined.

2.4 CREEP RATCHETING ANALYSIS

Because of the large temperature dependence of yield strength at high temperature, the thermal ratchet procedure has to reflect the temperature dependence of yield strength precisely. One of the thermal ratchet design procedures recommended in the Case 1592-11 does not appear to be applicable at the temperature where yield strength is strongly temperature dependent.

The method of the test No. 3 originated from the investigation of O'Donnell and Porowski. The method stands on the fact that in the shake-down region S_1 and S_2 and the plastic shake-down region P, there is an elastic core at the middle part of the plate where no plastic deformation will occur during the entire thermal cycle. The stress in the elastic core, σ_c, is simply determined by the yield strength of shut-down temperature σ^L_y. Figure 8 shows the stress distributions during a thermal cycle for the stress conditions of S_2. The stress distributions shown in the second and third row of Fig. 8 are the stress histories for the cases when the yield stress at the operating temperatures is lower than the yield strength at the shut-down temperature.

In all cases of the S_1, S_2, and P, it can be shown that the ratchet strain will occur if the following condition is met:

$$\sigma_c > \sigma_y' \qquad (1)$$

where the value σ_y' is the yield strength of the metal at the operating temperature.

That is, although the core stress is determined uniquely by the low temperature yield strength, the ratchet boundary is determined by the yield strengthes of both shut-down and operating temperature. From the Equation 1 , the ratchet boundary is given by the following equations:

$$\sigma_y' = (\sigma_t + \sigma^L_y) - 2\sigma_t(\sigma^L_y - \sigma_p) \quad \text{..... for } S_1 \text{ region} \qquad (2)$$

$$\sigma_y' = \sigma_p\sigma_t/\sigma^L_y \quad \text{..... for } S_2 \text{ and P regions} \qquad (3)$$

where the values σ_p and σ_t are the primary and secondary stresses.
This ratchet boundary was compared with that given in the Code Case 1592 and Case 1592-8 in Fig. 9. The dotted curves are the corrected boundaries of Eqs. 2 and 3 , and the heavy curve is the ratchet boundary described in the Case 1592. These two sets of the boundaries were shown for the case that the yield strength at the operating temperature, σ_y', is one half of the yield strength at the shut-down temperature, σ^L_y.

In order to limit the usage of the test No. 3 into the non-ratchet region in the new code, following sentences were added to sentences of the Code Case 1592-8.

"The upper bound to be allowed in test No. 3 is represented by the equation.

$$z = z_{1limit}$$

were z_{1limit} is the ratio of the yield strengths at the higher and lower of the wall-averaged temperatures for the stress extremes defining the secondary stress range Q_R".

2.5 CREEP-FATIGUE INTERACTION

The fatigue properties are one of our concerns. The figure 10 shows the environmental effect on the fatigue lives of Inconel 617. The fatigue life increased in the helium gas, which is considered to be partly due to decarburization and partly due to the inert atmosphere. When the material is carburized, the fatigue life was found to decrease slightly.

Many methods for the prediction of the creep-fatigue interaction lives had been proposed in literature. We are still studying which method is the best for the prediction of fatigue life of Inconel 617. Figure 11 shows an example of the fatigue lives of Inconel 617 under the strain hold conditions. It is seen that fatigue lives decreases with the increase of strain hold time. Figure 12 shows the effect of wave form on the fatigue lives. The tensile strain hold time most decreases the lives.

The results of analysis by linear-creep fatigue interaction rule are shown in Fig. 13 and the results imply that the linear-creep-fatigue rules predicts lives conservatively.

The creep damage was calculated by the time ratio in this analysis, and the fatigue damage was calculated by cycle ratio. The results imply that the creep damage calculated by time ratio gives conservative estimation of time-dependent damage.

Based on these observations, the creep-fatigue interaction is evaluated using this linear creep fatigue interaction rule in our design guide.

FATIGUE DESIGN CURVES FOR ELASTIC ANALYSIS

Fatigue Design Curves for in-elastic analysis was determined either by deviding the average lives by a factor of 20, or by deviding the strain amplitude by 2.

Fatigue Design Curves for elastic analysis was obtained by the following procedure.

To simplify the explanation, the creep fatigue damages of the notched components with and without hold time may be considered. The creep-fatigue damage of the notched component can be devided into three parts, namely pure fatigue damage, creep damage due to nominal stress, and creep damage due to peak stress. The hold time, which simulates the steady operation of system, increases the fatigue damage by increasing the strain amplitude during hold time. The hold time should increase also the creep damage due to peak stress which continues relaxing during the hold time. Because it is impractical to analyse the creep relaxation curves at design stage, it was decided to estimate the maximum creep damage due to peak stress and to include that maximum creep damage into the fatigue design curves for elastic analysis.

Figure 14 shows the creep damage calculated as a function of hold time. These curves were obtained from the creep rupture data and the relaxation curves during strain hold time of smooth specimen fatigue tests. In Fig. 14, creep damage is seen to approach the plateau values with increase of the hold time. The plateau value was considered as the maximum creep damage for each strain amplitude.

Using the linear creep-fatigue damage rule, this maximum creep damage was added to the average fatigue life curve and the minimum fatigue life curve was obtained. The results were compared with the experimental lives in Fig. 15 which proves that the predicted minimum fatigue life curve is lower than all the experimental fatigue lives with hold time. The design fatigue curves for elastic analysis were obtained by adding this maximum creep damage to the fatigue design curve for inelastic analysis.

2.6 TERTIARY-CREEP-DOMINATED CREEP CURVES

Figure 16 illustrates typical creep curves of the Inconel 617 at 1000°C. It is seen that unlike the creep curves at the elevated temperatures, the tertiary stage of the creep curves of these alloys at high temperatures often starts very early in the life. This is believed to be due to the metallurgical instability of the alloys at the high temperatures.

Early start of tertiary creep may affect a couple of sections in the strength design code; namely the determination of the S_t values and the design time for the creep buclking. If one uses the tertiary creep strength for the determination of the S_t values in the similar manner to the CC 1592, the S_t values may turn out to be impractically small value. However, the early onset of the accelerated creep in Inconel 617 is considered to be different from the tertiary creep onset at the elevated temperatures, because this accelerated creep period is often followed by the steady creep period and because a very long time and a large deformation have to be experienced before the actual fracture occurs. Therefore, an alternative method to determine the S_t values should replace the tertiary creep strength in the cc 1592 at the high temperatures. We are investigating the following material properties as the condidate properties to be replaced the tertiary creep strength; 1) true tertiary creep strength, 2) void formation strength, and 3) a strength related to the creep rupture ductility.

In the creep buckling analysis, the early onset of tertiary creep enhanced the onset of creep buckling. Figure 17 compares the calculated creep buckling lives of columns as a function of the applied stress. The creep curves used in the analysis were of two types; namely one is creep curves consisted of only steady creep region and the other is a set of creep curves consisted of steady and accelerated creep regions.

3. CLOSING REMARKS

Background experiments of a design code for 1.5 MWt high temperature helium heat exchanger were described. The experimental program is consisted of material strength tests and model tests. Because the space is limited, only a part of the experimental works which are related the determination of design stress intensities were described in this paper.

ACKNOWLEDGEMENT

This work was conducted as part of "Research and Development of Direct Steel Making Technology by Utilizing High Temperature Reduced Gas", which is one of the National Research and Development Program by Agency of Industrial Science and Technology, Ministry of International Trade and Industries.

TABLE I

Experiment Works for Establishing the Design Code for 1.5 Mwt Helium Heat Exchanger System

Material Properties (Deformation Fracture Strength)

- Short Time Tensile
- Creep and Relaxation
- Creep - Fatigue Interaction
- Crack Propagation
- Tribology (Wear , Selfwelding Fretting)

Helium Effect { Carburization / Decarburization
Weld
Cold Work
Biaxiality (Internal Press , Tension-Torsion)
Heat Treatment
Aging

Model Tests

- Creep of Notched Members
- Creep-Fatigue of Notched Members
- "Nozzle" Models
- "Center Pipe with Tubes" Model

Buckling & Creep Buckling

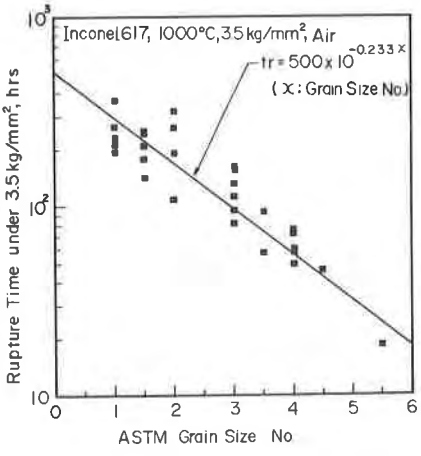

Fig. 1 A Relationship between Creep Rupture Time and Grain Size of Inconel 617

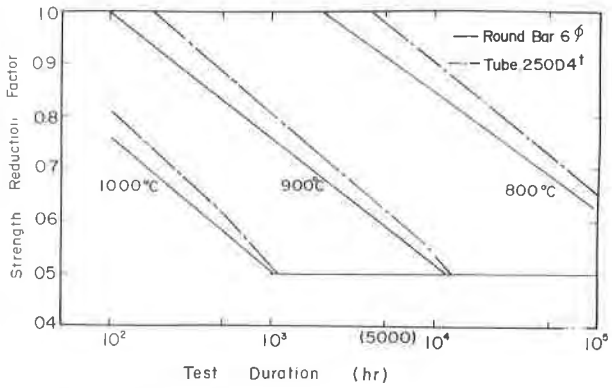

Fig. 2 Strength Reduction Factor Associated with Impure Helium Atmosphere

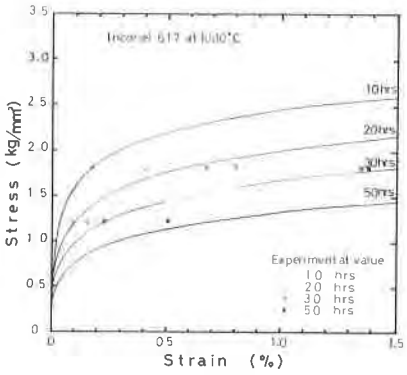

Fig. 3 Isochronous Stress Strain Curues in 99,995% He at 1000°C

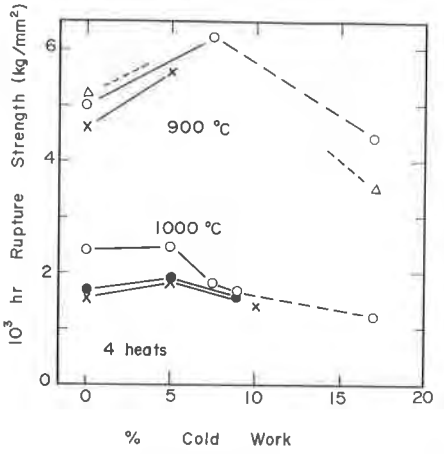

Fig. 4 The Effect of Cold Work on the Creep Rupture Strength of Inconel 617

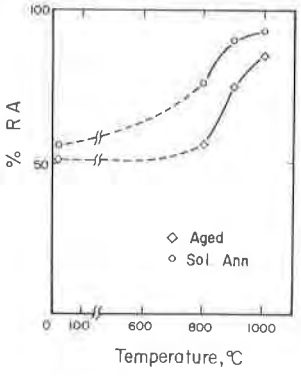

Fig. 5 Tensile Ductility of Inconel 617 solution annealed and aged for 3000 hrs at 1000°C

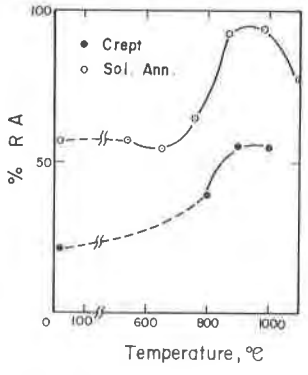

Fig. 6 Tensile Ductility of Inconel 617 solution annealed and crept for 1000 hrs at 1000 C under 1.5 kg/mm²

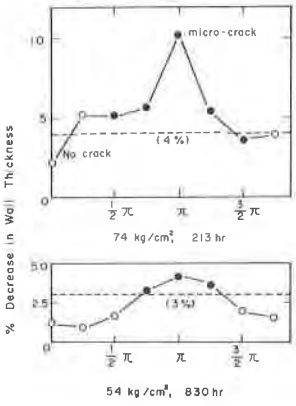

Fig. 7 The Strain Distribution along the Circumference of Creep Ruptured Inconel 617

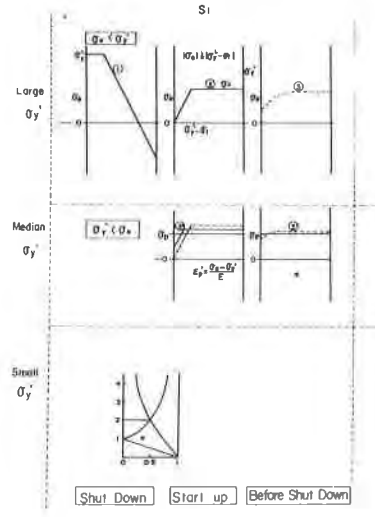

Fig. 8 Stress Distribution in tube Wall during a Thermal Cycle (Shake-Down Region S_2)

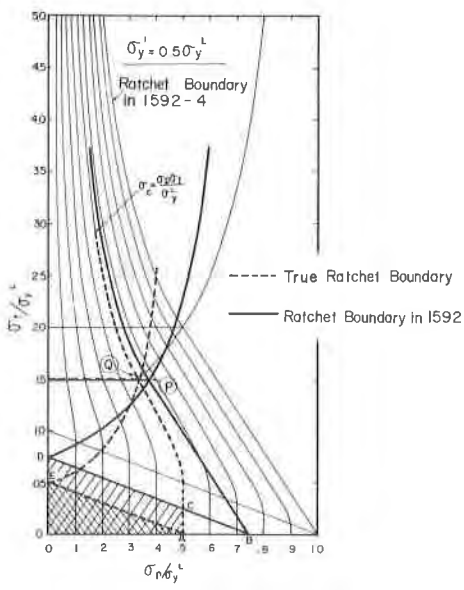

Fig. 9 Thermal Ratchet Limits in Code Case 1592, and 1592-4

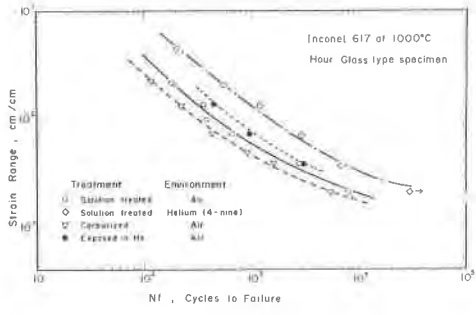

Fig. 10 Low-cycle Fatigue Life of Solution Treated and Carbulized Inconel 617 at 1000 C in Air and 4-nine Helium

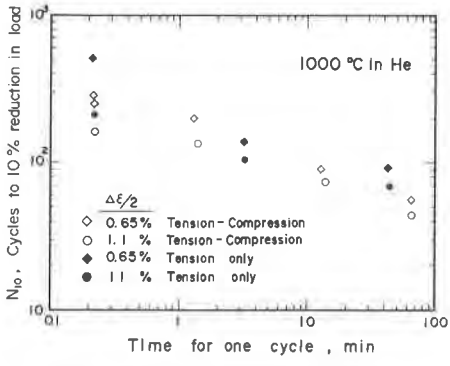

Fig. 11 Influence of hold time on fatigue life of Inconel 617 at 1,000°C in helium

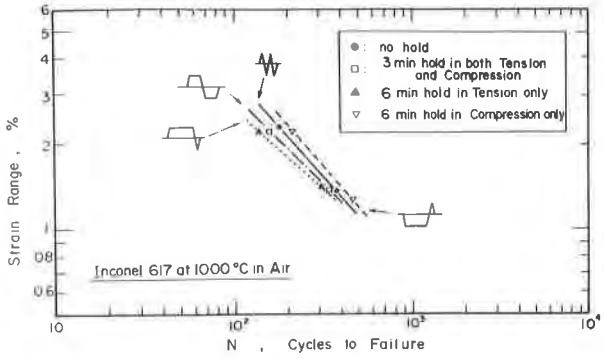

Fig. 12 Effect of Hold Time and Strain Wave Form on Low-Cycle Fatigue Life of Inconel 617 at 1000°C in Air

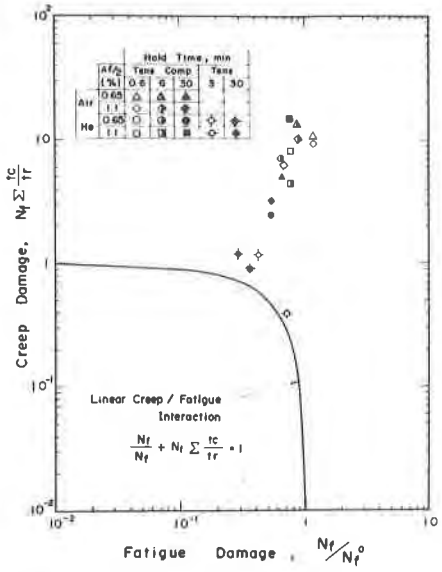

Fig. 13 Comparison of calculated damage life fraction with the linear creep-fatigue interaction rule

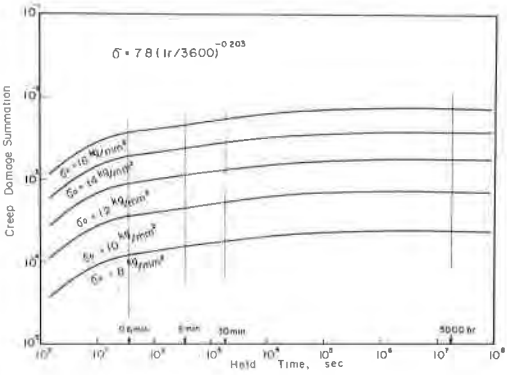

Fig. 14 Estimated Creep Damage as a Function of Hold Time

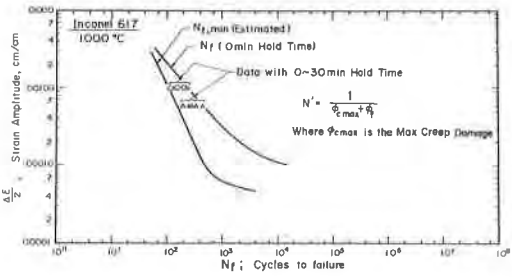

Fig. 15 Estimated Maximum Effect of Hold Time on the Fatigue Life of Inconel 617

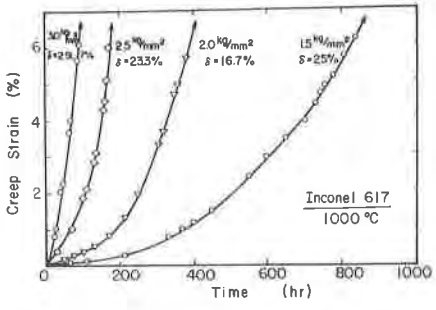

Fig. 16 Typical Creep Curves of Inconel 617 at 1000°C

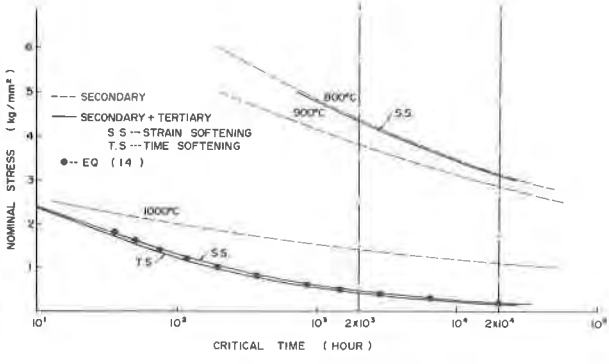

Fig. 17 Stress vs. Critical Time for the Column under Axial Compression